tvst

https://doi.org/10.1167/tvst.8.5.12

Article

Fluorescence Lifetime Imaging Ophthalmoscopy of the Retinal Pigment Epithelium During Wound Healing After Laser Irradiation

Alessa Hutfilz[1,3], Svenja Rebecca Sonntag[2], Britta Lewke[1,3], Dirk Theisen-Kunde[3], Salvatore Grisanti[2], Ralf Brinkmann[1,3], and Yoko Miura[1–3]

[1] Institute of Biomedical Optics, University of Lübeck, Lübeck, Germany
[2] Department of Ophthalmology, University Hospital Schleswig-Holstein, Campus Lübeck, Lübeck, Germany
[3] Medical Laser Center Lübeck, Lübeck, Germany

Correspondence: Yoko Miura, Institute of Biomedical Optics, University of Lübeck, Peter-Monnik-Weg 4, 23562 Lübeck, Germany. e-mail: miura@bmo.uni-luebeck.de

Received: 4 December 2018
Accepted: 19 June 2019
Published: 18 September 2019

Keywords: retinal pigment epithelium; fluorescence lifetime; selective retina therapy; wound healing; energy metabolism

Citation: Hutfilz A, Sonntag SR, Lewke B, Theisen-Kunde D, Grisanti S, Brinkmann R, Miura Y. Fluorescence lifetime imaging ophthalmoscopy of the retinal pigment epithelium during wound healing after laser irradiation. Trans Vis Sci Tech. 2019;8(5):12, https://doi.org/10.1167/tvst.8.5.12

Purpose: To investigate the change in fluorescence lifetime of retinal pigment epithelium (RPE) after laser irradiation by using an organ culture model.

Methods: Porcine RPE-choroid-sclera explants were irradiated with selective retina treatment laser (wavelength: 527 nm, beam diameter: 200 μm, energy: 80–150 μJ). At 24 and 72 hours after irradiation, the mean fluorescence lifetime (τ_m) was measured with fluorescence lifetime imaging ophthalmoscopy (FLIO) (excitation wavelength: 473 nm, emission: short spectral channel: 498-560 nm, long spectral channel: 560–720 nm). For every laser spot, central damaged zone (zone 1: 120 × 120 μm), area including wound rim (280 × 280 μm except zone 1), and environmental zone (440 × 440 μm except zone 1 and 2) were analyzed. Peripheral zone at a distance from laser spots longer than 2000 μm was examined for comparison. Cell viability was evaluated with calcein-acetoxymethyl ester and morphology with fluorescence microscopy for filamentous-actin.

Results: The RPE defect after selective retina treatment was mostly closed within 72 hours. FLIO clearly demarcated the irradiated region, with prolonged τ_m at the center of the defect decreasing with eccentricity. In short spectral channel, but not in long spectral channel, τ_m in the environmental zone after 72 hours was still significantly longer than in the peripheral zone.

Conclusions: FLIO may clearly demarcate the RPE defect, demonstrate its closure, and, moreover, indicate the induced metabolic changes of surrounding cells during wound healing.

Translational Relevance: This ex vivo study showed that FLIO may be used to evaluate the extent and quality of restoration of the damaged RPE and to detect its metabolic change in human fundus noninvasively.

Introduction

The retinal pigment epithelium (RPE), a monolayered epithelium at the most outside of the retina, forms the outer blood retina barrier, and plays a crucial role in maintaining retinal homeostasis.[1,2] The metabolic state of the RPE is essentially linked to the retinal function, and its decline may lead to the pathogenesis of different chorioretinal diseases.[3,4] Therefore, a sensitive diagnostic approach that may detect not only structural but also metabolic changes of the RPE is desired.

Fluorescence lifetime imaging ophthalmoscopy (FLIO) is a new diagnostic tool, which measures the fluorescence lifetime (FLT) of the fundus.[5–7] FLT is one of the fluorophore-specific properties, defined as the time duration until the fluorescence intensity drops down to 1/e (about 36%) of the initial value after exciting a fluorophore with short-pulsed light.[8] FLT is assumed to be an intensity-independent value

and has the potential to detect changes in fluorescent compounds in observed tissues. There are different natural fluorophores in fundus tissues, including the well-known lipofuscin.[9] Also, structural proteins, such as collagen and elastin,[5] melanin,[5] and advanced glycation endproducts (AGE)[5] or metabolic coenzymes like flavin adenine dinucleotide (FAD),[10] have fluorescent properties. Therefore, not only structural but also metabolic alterations may cause a change in the distribution and concentration of fluorophores in tissue. This consequently leads to an alteration of FLT. FLIO uses a repetitive picosecond pulsed scanning laser of 473-nm wavelength for excitation. The FLT of detected autofluorescence (AF) in fundus tissues with wavelengths ranging from 498 to 560 nm (short spectral channel, SSC) and 560 to 720 nm (long spectral channel, LSC) are mapped as pseudocolor image.

Several clinical pilot studies have shown that FLIO might be useful to differentiate subretinal deposits with different components,[11] indicate the amount of macular pigments,[12,13] as well as clearly demarcate RPE atrophy area.[14,15] Moreover, it was shown that FLIO has the potential to differentiate retinae with metabolic disturbance from the healthy ones; for example, retinae of diabetic patients without retinopathy,[16] those with a very early stage of age-related macular degeneration (AMD),[15,17] or macular telangiectasia.[18] These results demonstrate the great potential of FLIO, but the basic understanding about FLTs of fundus tissues under physiological as well as pathological conditions are still quite limited.[5]

Wound healing of the RPE is essential to maintain or restore the function of the RPE itself and eventually also of the retina. Therefore, RPE response to injury is one of the good indicators of RPE health. Wound closure, achieved by different cell functions such as migration and proliferation, must be accompanied by the activation of cell metabolism. As one of the therapeutic mechanisms of retinal laser treatment, enhancement of the metabolic activity of the RPE and eventually of the retina is suggested.[19–21] However, this has not yet directly been proven. The metabolic cofactor FAD is known to show different FLTs depending on its protein-binding states (free form or protein-bound form).[10] This protein-binding state, namely the ratio of protein bound to free FAD, may be changed according to the status of cellular energy metabolism. FLIO is expected to be able to indicate the status change of FAD, showing the change in the energy metabolic state.

Based on these backgrounds, we aimed to investigate the FLTs of the RPE during wound healing to elucidate FLT changes in FLIO with morphological and metabolic alterations of the RPE. This could be useful to understand the full potential of FLIO.

To create a cell defect within the RPE, we used a laser for selective retina treatment (SRT). SRT enables selective destruction of the RPE through microbubble formation around the melanosomes. It uses multiple microsecond laser pulses shorter than the thermal confinement with low repetition rates.[22–27] The clinical effectiveness of SRT has previously been reported for the treatment of central serous chorioretinopathy[28,29] and diabetic macular edema.[30] In contrast to photocoagulation laser, SRT does not have a thermal impact around the damaged RPE cells.[22] This enables the creation of a local defect with clear border,[22,28–30] followed by the wound closure through migration and proliferation of surrounding RPE cells.[31]

In this study, we used FLIO to investigate the FLTs of ex vivo RPE during wound healing after SRT laser irradiation. Although the main purpose of this study was to monitor the wound healing of RPE with FLIO, this study may also enhance the essential understanding of the FLTs of the RPE and the choroid.

Materials and Methods

RPE-Choroid-Sclera Culture

Freshly enucleated porcine eyes were used in this study. After removing the extraocular tissues and immersing the eyes in an antiseptic solution (betaisodona, 2% povidone-iodine; Mundipharma GmbH, Limburg, Germany), the anterior parts of the eye, the lens, and the vitreous body were removed, and the neural retina was gently detached from the RPE. The RPE-choroid-sclera explant was then resected from the posterior eye cup by using a trepan with a diameter of 12 mm. The RPE-choroid-sclera explant was then cultivated in a Dulbecco's modified Eagle medium (DMEM; high glucose; Merck KgaA, Darmstadt, Germany) supplemented with 10% porcine serum, 1 mM sodium pyruvate, and antibiotic antimycotic, in a 5% CO_2 incubator at 37°C.

SRT Laser Irradiation

The RPE of the explant was irradiated by the SRT-Laser (Medical Laser Center Lübeck, Lübeck,

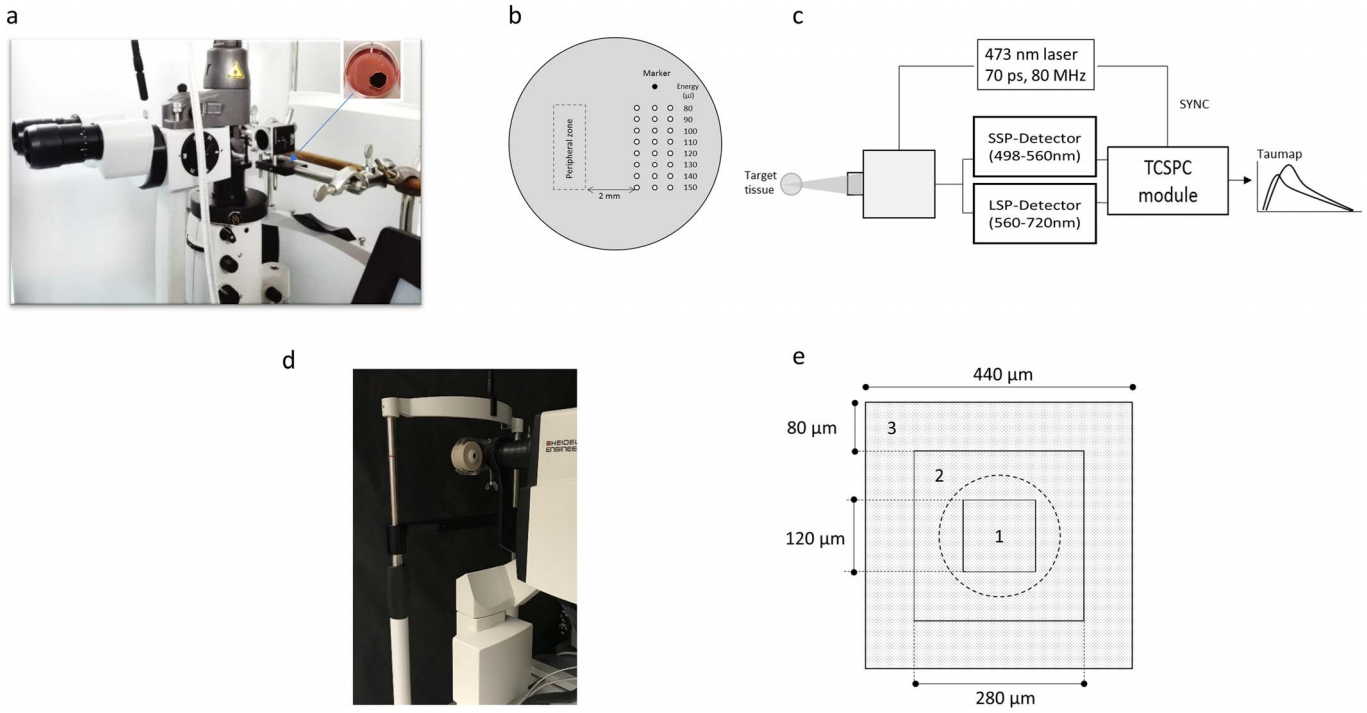

Figure 1. SRT laser irradiation and FLIO on RPE-choroid-sclera explants. (a) Setup for SRT laser irradiation of the RPE explant: a turning mirror and a horizontal stage fixed in front of the slit lamp enables the laser irradiation on the tissue placed in the culture medium in the dish (presented in the zoomed picture in the *upper-right* corner). (b) A schematic drawing of the pattern of SRT laser irradiation. (c) A schematic drawing of the FLIO system: the tissue is excited at 473 nm with a pulsed picosecond laser and the emitted fluorescence light is spectrally detected by two hybrid photon-counting detectors; SSP, short spectrum; LS, long spectrum; TCSPC, time-correlated single-photon counting. (d) FLIO on the ex vivo RPE using a custom-made chamber. (e) Zones for the FLT analysis at/around a laser spot: (1) the central zone with 120 × 120 µm (zone 1), (2) the adjacent surrounding up to 280 × 280 µm (zone 2) excluding zone 1, and (3) the area up to 440 × 440 µm excluding zone 1 and zone 2 (zone 3). The area of the laser beam (200-µm diameter) is shown with a *circle* at the center.

Germany) 24 hours after tissue isolation. The setup consists of a slit-lamp-adapted, frequency-doubled Nd:YFL laser with a wavelength of 527 nm and a pulse duration of 1.7 µs. A turning mirror (CCM1-P01/M; Thorlabs, Newton, NJ) and a horizontal stage were fixed in front of the slit lamp, so that the RPE explant could be irradiated in the culture dish (Fig. 1a). One exposition of SRT laser irradiation consists of 30 pulses with a repetition rate of 100 Hz. A beam spot diameter was 200 µm. The laser pulse energy for irradiation was from 80 µJ to 150 µJ with increments of 10 µJ. For the orientation, a marker irradiation was applied with 150 µJ, and 3 repeated lines of irradiation with the series of energy were applied on each explant with the spot interval of more than 200 µm (Fig. 1b). After laser irradiation, the explants were placed back into the incubator and maintained until FLIO was performed at the indicated points in time (24 and 72 hours after irradiation).

Fluorescence Lifetime Imaging Ophthalmoscopy

FLT imaging of the RPE on the explant was performed by a FLIO system, a prototype provided by Heidelberg Engineering GmbH (Heidelberg, Germany) 24 and 72 hours after laser irradiation. The schematic description of the setup is shown in Figure 1c. For the FLIO measurement, the RPE-choroid-sclera explant was placed in a custom-made chamber filled with Dulbecco's phosphate-buffered saline without calcium and magnesium (PBS [–]), which was then fixed in front of the FLIO device (Fig. 1d). For excitation, the object was raster scanned by a pulsed (70 ps) diode laser radiation of 473-nm wavelength with an 80-MHz repetition rate at a frame rate of 9 Hz. A 30° field was analyzed, imaging the entire tissue section. Highly sensitive hybrid photon-counting detectors (HPM-100-40; Becker& Hickl GmbH, Berlin, Germany) detect the emitted photons in two spectral channels of 498 to 560 nm

(SSC) and 560 to 720 nm (LSC). The detector signals were registered by means of time-correlated single photon counting modules (SPC-150; Becker&Hickl GmbH), and the acquired lifetime data of the 256 × 256 pixels were analyzed by SPCImage 6.4 software (Becker&Hickl GmbH). For analysis, the fluorescence decay at each pixel was fitted to a biexponential curve without pixel binning. The total function of the FLT is the sum of each exponential components;

$$f(t) = a_1 \times e^{-t/\tau_1} + a_2 \times e^{-t/\tau_2}, \quad (1)$$

where τ_1 and τ_2 indicate the FLTs of the short and long exponential components, respectively, and a_1 and a_2 their respective amplitudes.

The mean FLT (τ_m) is defined by

$$\tau_m = \frac{a_1 \times \tau_1 + a_2 \times \tau_2}{a_1 + a_2}. \quad (2)$$

A decay matrix calculation with SPCImage creates a pseudocolored image of the examined parameter. This series of procedures is conducted for both spectral channels.

Analysis of FLT at/around the Laser Spots

For every laser spot, the FLIO parameters (τ_1, τ_2, a_1, a_2) from a section of 20 × 20 pixels (about 800 µm × 800 µm) centered at the laser spot were exported from SPCImage software to Microsoft Excel 2016. τ_m was calculated from these parameters with the formula shown in equation 2. The three different zones were defined and investigated: zone 1 as the central zone of 120 × 120 µm, zone 2 as the adjacent surrounding up to 280 × 280 µm excluding zone 1, and zone 3 as the area up to 440 × 440 µm excluding zone 1 and zone 2 (Fig. 1e). The peripheral zone, defined as the area of 20 × 20 pixels at a distance greater than 2000 mm from the last raw of laser spots within the same explant, was used for comparison. Four different areas within this zone were randomly selected for each explant and used for analysis.

Calcein-Acetoxymethyl Ester (AM) Viability Test

The viability of explant RPE cells were tested by calcein-AM directly after laser irradiation on samples different from the ones used for FLT measurements. Nonfluorescent calcein-AM diffuses into the cells and is converted to the fluorescent calcein by cytosolic esterase. Calcein fluoresces green by blue light excitation. Dead cells show no fluorescence. Explants were incubated with 5 µM calcein-AM (Thermo Fisher Scientific, Waltham, MA) in the PBS (–) for 15 minutes at 37°C, washed with PBS (–), and fluorescence microscopy was performed. A fluorescence microscope (Eclipse Ti-E; Nikon, Tokyo, Japan) with a fluorescein isothiocyanate (FITC) filter (excitation wavelength of 465–495 nm, dichroic mirror for 505 nm, and a barrier filter for 515–555 nm) was used.

Filamentous Actin (F-Actin) Staining

In order to confirm the wound healing response of the RPE at irradiated site, the morphology of RPE cells was visualized by the staining of the cytoskeleton, F-actin. The explants different from the ones used for FLT measurement were used for assessment. The explants were washed shortly with PBS (–) and fixed with 4% buffered formaldehyde (Roti-Histofix 4%; Carl Roth GmbH and Co., KG, Karlsruhe, Germany) for 10 minutes at room temperature. After washing with PBS (–) three times, the cells were permeabilized with 0.5% Triton-X 100 in PBS (–) for 10 minutes at room temperature. The explants were then again washed with PBS (–) three times and incubated with 1 µM FITC-phalloidin (Thermo Fisher Scientific) for 60 minutes at room temperature. After washing with PBS (–) three times, the explant was placed on the slide glass with the RPE side down with a mounting solution (SlowFade antifade mountant; Thermo Fisher Scientific) and observed with the fluorescence microscope (Nikon Eclipse Ti-E) using a FITC filter.

Statistical Data Analysis

SRT irradiation on one explant was conducted with three spots for each energy setting, and experiments were repeated more than three times. The statistical analysis was performed using GraphPad Prism version 7.04 (GraphPad Software, Inc., La Jolla, CA).

The Mann-Whitney *U* test was used for comparison of two groups. The comparison of more than two groups were performed by analysis of variance followed by a Dunnett's multiple comparison test because the normality was given for all groups. Normality was proved by the D'Agostino and Pearson normality test, while homogeneity of variance was tested by Brown-Forsythe test.

For the correlation between laser pulse energy (E_p) and the FLIO parameter, the correlation coefficient r was calculated by Pearson correlation analysis.

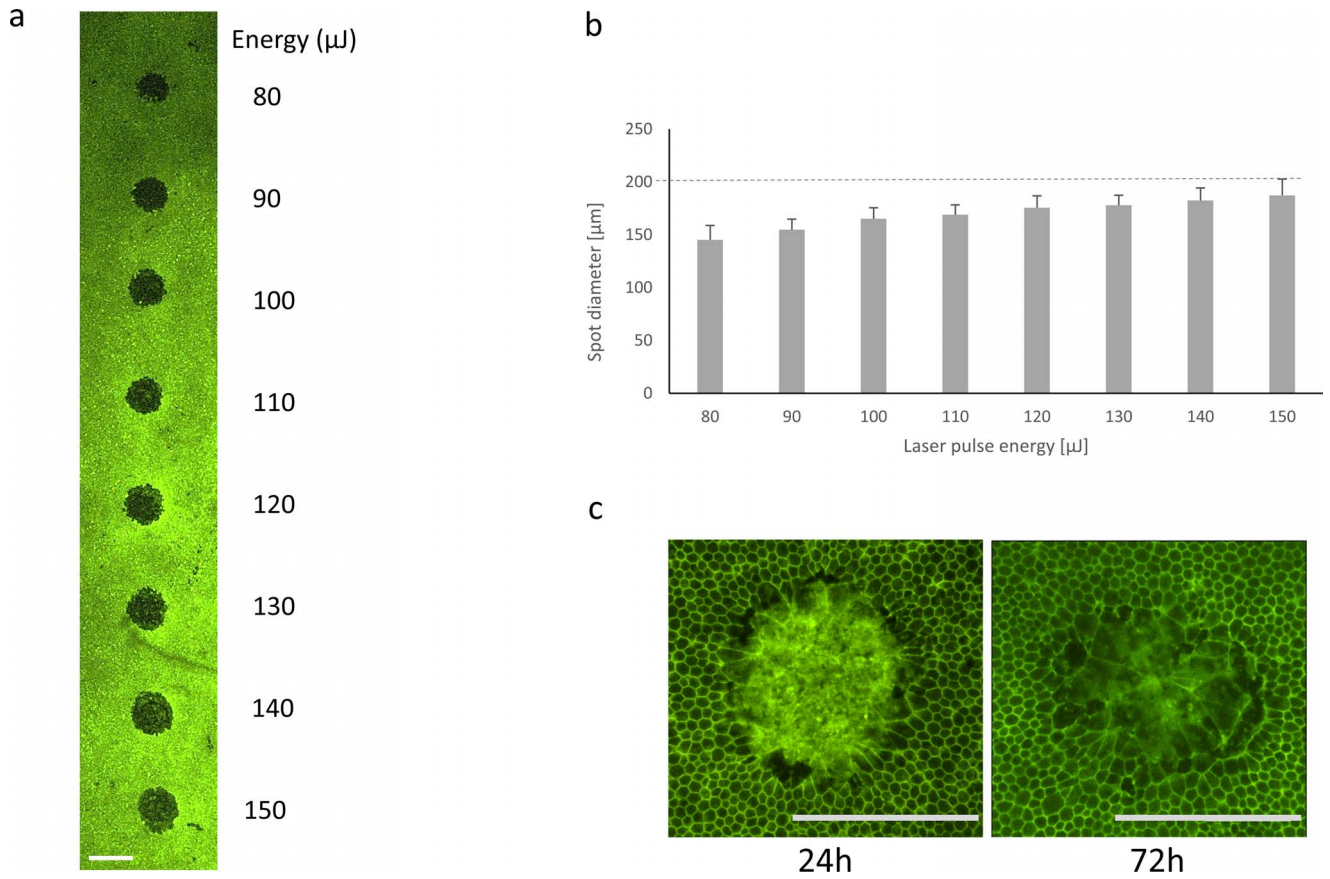

Figure 2. (a) Calcein-AM staining directly after irradiation with laser pulse energy ranged from 80 to 150 µm. The dead RPE area is shown as a nonfluorescent dark round spot. *Scale bar* = 200 µm. (b) Diameters of the damaged area directly after irradiation for different energies according to the calcein-AM test. (c) FITC-phalloidin staining at 24 (*left*) and 72 hours (*right*) after irradiation to visualize F-actin cytoskeleton: elongated RPE cells are observed typically after 24 hours at the wound rim. The central area is with debris of destroyed cells and the Bruch's membrane behind can be partially visible. After 72 hours the wound is almost closed (*Bar* = 200 µm).

The proceeding was equal for all data. The α was 0.05 and $P < 0.05$ was indicated as significant.

Results

SRT Laser-Induced RPE Cell Damage and Wound Healing

The result of the calcein-AM test directly after laser irradiation showed the demarcated area of RPE cell death for all energy settings examined in the current study (Fig. 2a). The spot diameter (mean ± SD) ranged from 145 ± 14 µm (80 µJ) to 187 ± 15 µm (150 µJ) and increased energy dependently (Fig. 2b). At 24 and 72 hours after laser irradiation, F-actin staining presented the elongation of the cells at the wound edge after 24 hours and the closure of the laser induced RPE gap after 72 hours (Fig. 2c). The stretched RPE cells were shown in the restorated region.

Fluorescence Lifetime Imaging Ophthalmoscopy

Comparison With the Intensity Image of AF

Figure 3 demonstrates exemplary images obtained from the measurement with FLIO, the grayscale intensity image of the AF, and the color-coded image of τ_m (ps) of explants after laser irradiation. On AF, typically the hypofluorescence was observed at the laser spots and this change became blurry over time in both channels. The color-coded image of τ_m may indicate the irradiated site more clearly than AF in most spots. In this study, the shorter τ_m is presented in orange, and the longer τ_m is in blue. At the center of the laser spot, where the RPE cells were destroyed, the τ_m was highly prolonged. Moreover, the color-coded

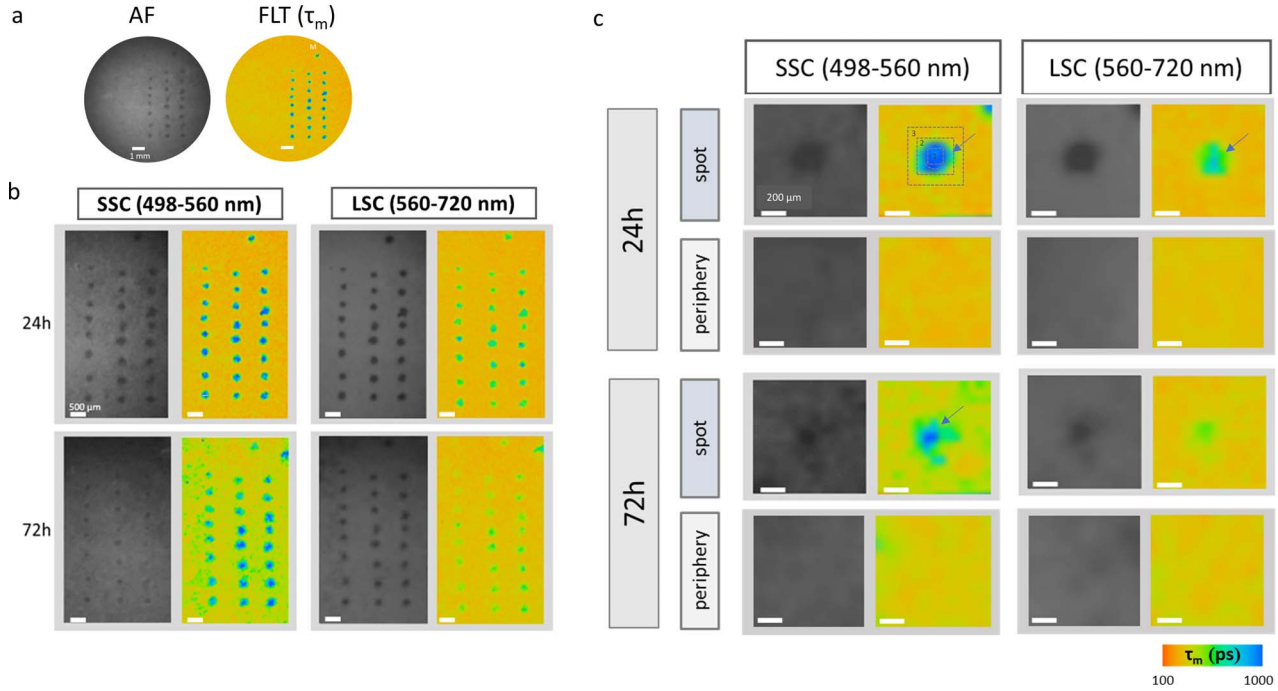

Figure 3. Exemplary images of AF intensity and color-coded τ_m in FLIO after laser irradiation. (a) Whole tissue image of AF intensity (*left*) and color-coded images of τ_m (*right*) at 24 hours after irradiation in the short spectral channel. (b) Zoomed images at the irradiated area in an explant after 24 and 72 hours. SSC, short spectral channel; LSC, long spectral channel. (c) Further zoomed images of AF intensity and color-coded τ_m at one laser spot area ("spot") and of one area of peripheral zone ("periphery") after 24 and 72 hours for both spectral channels. The *square* overlaid in the color-coded image of τ_m (*top, left*) shows the zones to be analyzed.

images of τ_m revealed the ring-shaped zone around the central defect area within the laser spots. The τ_m of this area was between the values of center and surroundings (Fig. 3c, arrows). This area cannot be differentiated in the AF intensity image.

Zone Analysis of FLT Parameters

In order to investigate the FLT at/around laser spots in detail, three different zones, defined as in Figure 1e, were separately analyzed.

In Figure 4, the box plots of τ_m calculated from all spots are presented. The median and 25% and 75% percentiles are shown in the table below each graph. The range between 25% and 75% percentiles of τ_m at peripheral zone for each point in time are also presented in the graph with colored horizontal bands (orange and green bands for 24 and 72 hours, respectively) and those values in the table below. The detailed analysis and interpretations are described in the following paragraphs.

Gradient of FLT at a Laser Spot (Zone 1 and 2). The graphs in Figure 4 clearly present a decreasing gradient of τ_m from zone 1 toward zone 3 at 24 and 72 hours in both channels. This change includes a laser-induced significant prolongation of τ_m in zone 1 and 2 in both channels compared to the values in the peripheral zone ($P < 0.0001$). The difference from peripheral zone is smaller in zone 2 compared to in zone 1, but there is still a significantly difference up to 72 hours.

In order to assess the changes over time (between 24 and 72 hours), the difference between the values in the examined zone and in peripheral zone of identical explant ($\Delta\tau_m$) was compared between both time points. According to this assessment, a decrease in τ_m in zone 1 from 24 hours to 72 hours was significant in both channels ($P < 0.05$).

FLT of the RPE Around a Laser Spot (Zone 3). Zone 3 is the area around a laser spot, where no cell death has occurred, but on the other hand, different kinds of sublethal secondary cellular responses for wound healing are supposed to be activated. In SSC, τ_m at this zone was significantly longer compared to peripheral zone at both points in time ($P < 0.01$ and $P < 0.05$ after 24 and 72 hours, respectively). In LSC, no significant differences from the value in the peripheral zone or between time points were found (Fig. 4b).

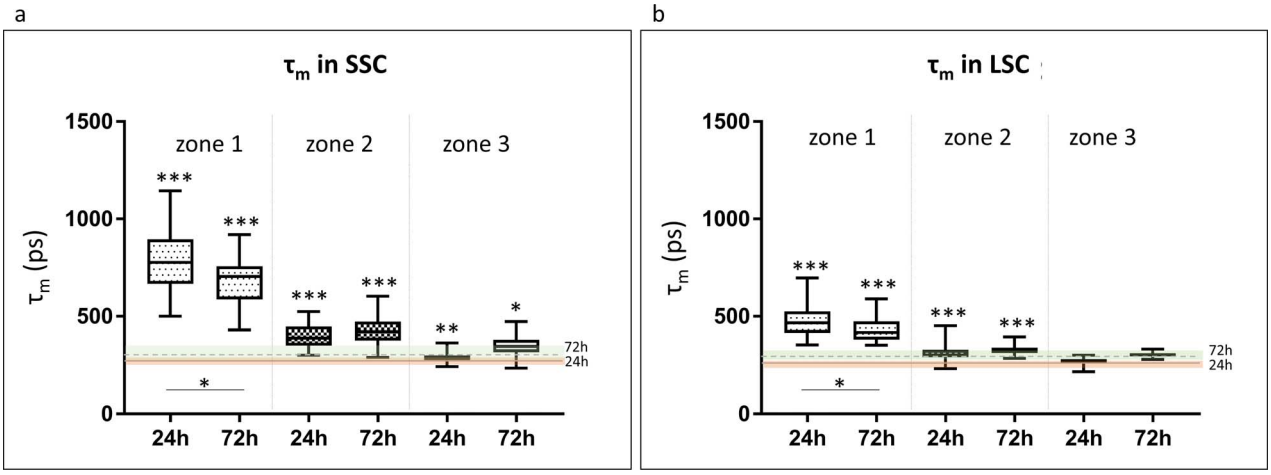

SSC (498-560 nm)		zone 1	zone 2	zone 3	periphery
24h	25% percentile	684	351	279	246
	median	777	390	285	262
	75% percentile	885	447	297	282
72h	25% percentile	587	383	320	270
	median	704	422	347	308
	75% percentile	756	473	377	354

LSC (560-720 nm)		zone 1	zone 2	zone 3	periphery
24h	25% percentile	418	292	258	242
	median	467	303	271	266
	75% percentile	520	326	281	272
72h	25% percentile	383	314	297	284
	median	418	327	305	297
	75% percentile	468	340	312	315

Figure 4. Boxplots for τ_m at laser spots after 24 and 72 hours in SSC (a) and LSC (b), indicating minimum (the end of the lower whisker), 25% percentile (the lower end of the box), median (the horizontal bar in the box), 75% percentile (the upper end of the box), and maximum (the end of the upper whisker). The range between 25% and 75% percentiles of τ_m at the peripheral zone for each point in time are presented with *colored horizontal bands* (*orange* and *green bands* for 24 and 72 hours, respectively). The tables under each graph show the values of 25% percentile, median, and 75% percentile for each point in time and zone. *** $P < 0.001$, ** $P < 0.01$, * $P < 0.05$; *asterisk* at boxes indicates the significance of difference from the value at peripheral zone at each point in time, and *asterisk* shown between 24 and 72 hours indicates the significance of difference in $\Delta\tau_m$ (difference from peripheral zone) between two time points.

Dependency of the FLT on the Irradiation Laser Pulse Energy

In Figure 5, τ_m at the spots are shown for different energies. As expected, the values in zone 1 and 2, where the defected area must be initially included, seem to have a slight energy dependency especially at the first several energy steps (e.g., from 80 µJ to 120 µJ) (Figs. 5a, 5b, 5d, 5e), which might be related to the increase in the spot size. In zone 3 there seems to be no difference among different energies (Figs. 5c, 5f). In Table 1, results of Pearson's correlation analysis are shown for laser pulse energy and the values of τ_m. In zone 1 and zone 2, as assumed from the graphs above, they all show a weak to mild correlation with laser pulse energy ($0.3 <$ |correlation coefficient: $r| < 0.7$). On the other hand, in zone 3, almost no values have an energy dependency, where a weak positive correlation with energy was shown for τ_m in LSC. Overall, the energy dependency of τ_m for the range of 80 to 150 µJ was not high, and the descriptions stated in the upper two paragraphs apply in general.

Discussion

In this study, we conducted a detailed analysis of the FLT with FLIO at and around laser spots using ex vivo RPE-choroid-sclera explants. This is a good model to simulate FLIO and investigate the FLT after laser-induced damage and subsequent wound healing of the RPE.

The results of the current study showed that it is possible to perform an analysis of the RPE during wound healing with FLIO, which provides additional information on the AF intensity measurement. AF intensity images highlight mainly the lipofuscin distribution and concentration in fundus due to its high fluorescence intensity.[32–34] FLTs, which are assume to be independent of the AF intensity, indicate the existence of fluorophores other than lipofuscin.

Major fluorophores in RPE-choroid tissues known to date are lipofuscin (different bisretinoids including A2E), AGE, melanin, FAD, collagen, and elastin. Considering the spectral characteristic, the peak of

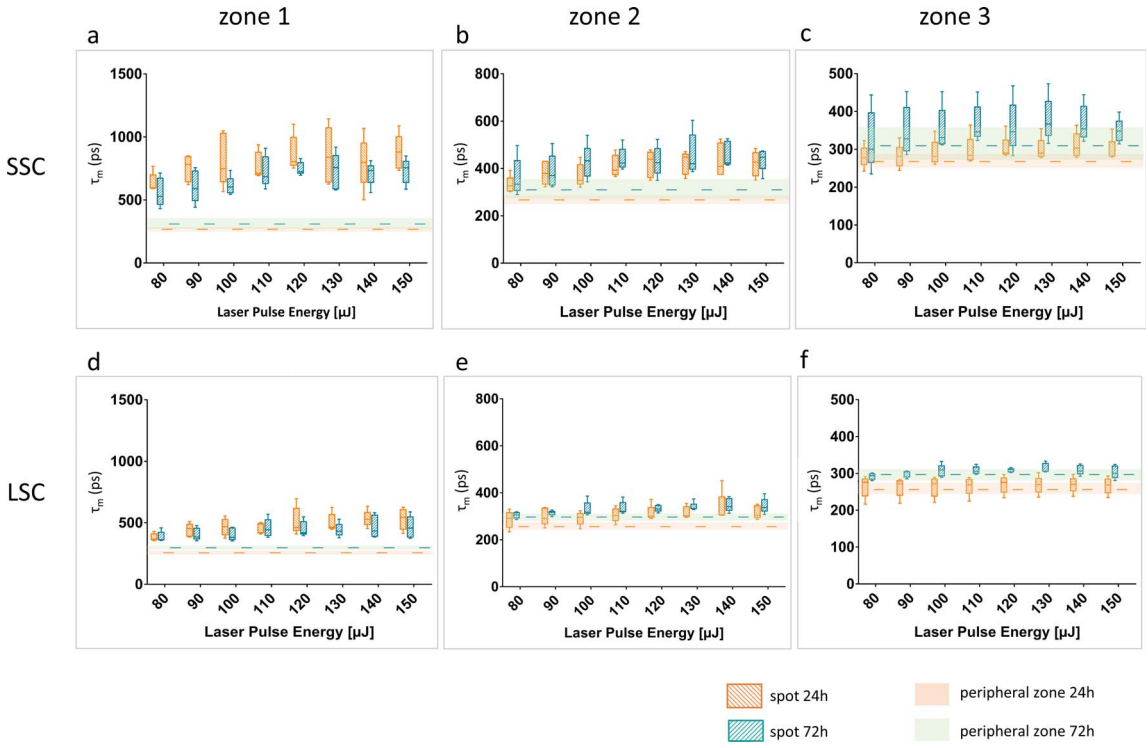

Figure 5. τ_m at/around laser spots for different pulse energies. τ_m for different pulse energies in both channels after 24 (*orange*) and 72 hours (*green*). The values at peripheral zone are given as in Figure 4.

emission wavelength (λ_{em}) of lipofuscin is around 590 nm when excited by 480 nm, whereas A2E shows its emission peak around 630 nm.[33] The λ_{em} of AGE lies at 523 nm when excited by 470 nm.[5] The impact of melanin fluorescence in FLIO is still under discussion: melanin shows a weak AF at excitations longer than 400 nm and here it shows strong absorption. However, according to a report by Kayaz et al.,[35] oxidized melanin may be fluorescent with an emission peak around 540 nm under 470-nm excitation. However, the extent of oxidation of RPE-melanosomes in the examined tissues remains unclear, and it needs to be further investigated. The spectrum of λ_{em} of FAD lies between 500 and 565 nm with a maximum at 524 nm when excited at 470 nm.[5] Collagen shows very weak AF at the excitation with 470-nm wavelength light. Collagen II, which shows the strongest absorption among collagen I to IV, has the emission maximal around 510 nm.[5] Based on those reported emission properties, the SSC (498–560 nm) of the FLIO is considered to be more sensitive to the changes in melanin, AGE, FAD, and collagen, whereas the LSC (560–720 nm) might be more sensitive to A2E and lipofuscin.

In the investigated fundus tissues, RPE has short FLTs; this could mainly due to numerous intracellu-

Table 1. Results of Pearson's Correlations Analysis (Correlation Coefficient: *r*) for Laser Energy Dependency of τ_m Shown in Fig. 5

	Zone 1		Zone 2		Zone 3	
Parameter	24 h	72 h	24 h	72 h	24 h	72 h
τ_m (SSC)						
r	0.36	0.48	0.5	0.39	0.26	0.17
P	0.02	0.001	<0.001	0.01	0.1	0.29
τ_m (LSC)						
r	0.56	0.39	0.36	0.51	0.08	0.33
P	<0.001	0.01	0.02	0.001	0.63	0.04

lar melanosomes concentrated at the apical side of cells.[36,37] These short FLTs should be more apparent in porcine eyes, as these are mostly from young pigs containing only small amount of lipofuscin.[37] The RPE shows τ_m of around 200 to 250 ps with fresh ex vivo samples (unpublished data), which is consistent with the results of previous report by other researchers.[5] Lipofuscin has so far been reported to have a much longer τ_m over 1000 ps[5,38]; an increasing amount of it may, therefore, also increase the total τ_m of the RPE. The Bruch's membrane and the choroid are first visible after the RPE cells have been destroyed or defectively injured. These layers show long FLTs, probably due to the contribution of collagen and elastin with long τ_m.[5] According to our own measurements, τ_m of the region without RPE (removed by a fine brush) in porcine eyes is ranging from 550 to 700 ps (unpublished data). This may explain why a significantly longer τ_m is shown in zone 1 at 24 hours after irradiation. This finding can also be supported by clinical pilot studies showing the apparently long τ_m in the area of RPE atrophy in patients of geographic atrophy,[14,15] retinitis pigmentosa,[39] or choroideremia.[40]

During wound healing of the RPE in the current study, prolonged τ_m in the central region becomes shorter over time. However, it was still longer than the values in the peripheral zone even after 72 hours, at which the wound must be almost closed. This might have anatomical or metabolic reasons. Melanosomes are considered to be less concentrated in the restoring cells, which are widely spread in shape to cover the defect. Additionally, due to the activated metabolisms of those cells compared to the intact RPE cells, these differences may occur. We hypothesize that both factors are related to the longer FLTs in the central regions during wound healing.

On the other hand, changes in the FLTs around the wound without any cell morphological changes (zone 3) may be associated with the change in cellular metabolic activity. Those changes were significant in SSC in the current study, and this result may indicate that SSC might be more sensitive to detect sublethally activated RPE cells around a wound than LSC. As described above, FAD is a metabolic cofactor that is essential in energy metabolisms of cells,[41] which serves as an electron acceptor in complex II of the respiratory chain in the mitochondria, and is a cofactor for succinate dehydrogenase. FAD changes its FLT depending on its protein binding states, where free FAD has long FLTs (2300 ± 700 ps), and protein-bound FAD has short FLTs (monomeric form: 130 ± 20 ps, dimeric form: 40 ± 10 ps).[10] The prolongation of the FAD-τ_m may indicate a relative increase of free FAD (long FLT component, τ_2-FAD), or a relative decrease of protein-bound FAD (short FLT component,τ_1-FAD).[42–45] This may theoretically indicate the metabolic shift to glycolysis.[46]

Considering the cell responses following wound healing, the protein-binding state of FAD may be changed in the RPE cells along with the changes in energy metabolic states. This study showed a slight but significant elongation of τ_m around laser spots (zone 3), where no morphological changes were observed. If this is caused by the change in FAD protein-binding states, it could be interpreted that the free form of FAD increased, indicating a relative increase of glycolysis. In this case, it is also of interest that metabolic activation around a laser spot seems to need some time to develop and lasts long. In order to prove this, different FAD forms are currently being investigated at our laboratory.

The contribution of the neural retina cannot be ignored in the clinical application of FLIO. In the neural retina, macular pigments, which consist of the natural xanthophyll pigments lutein, meso-zeaxanthin, and zeaxanthin, reach their greatest concentrations at the center of the fovea, and their contribution in FLIO with human fundus is large. These xanthophyll have been shown to have very short FLTs,[12,13,47] which make the FLT of the central fovea significantly shorter than of the peripheral retina.[12,13] Because FLIO may count the photons from the whole layer of the retina through the RPE at once, the FLT of neural retina, especially of macular pigments, needs to be taken into consideration in clinical application of FLIO. Investigating only the RPE-choroid tissue in this study, thus, presents one of the limitations.

As for other limitations, this study has been conducted with a small number of ex vivo tissues in a static organ culture system. Even though ex vivo RPE cells are phenotypically much closer to in vivo ones compared to the RPE cells in cell culture,[48] the change in microcircumstances may affect cellular responses and higher variability could be seen in vivo.

Nevertheless, a study like this one focusing on the RPE is of great value to make progress in better understanding the RPE pathology-related FLT changes in human fundus. In the future, we plan to combine FLIO with biological assessments, such as the measurement of energy metabolic states. This will not be limited to the RPE but also will include the neural retina under different pathological conditions.

The results of the current study indicate that FLIO might be a sensitive method for monitoring wound healing of the RPE. Furthermore, FLIO may highlight concurrent metabolic alterations, which goes beyond conventional AF imaging. This is of interest for clinical ophthalmologists, as it indicates not only morphological changes based on the different FLT but also the early changes in the metabolisms and functional cell status within different tissues of the fundus. This could be applied to detect early changes in different chorioretinal diseases associated to the cellular metabolic changes, as well as to evaluate treatment effects. Furthermore, different laser treatments, such as panretinal or subvisible laser treatments, could also be followed with this method. It may be interesting to learn more about metabolic changes in these tissues after laser exposure.

Here, FLIO offers additional information to many other conventional modalities. Further basic and clinical research is certainly necessary to use and better understand FLIO in clinical practice.

Acknowledgments

This work was supported by BMBF (Federal Ministry of Education and Research in Germany), grant numbers 13N14444 and 13N14445.

Disclosure: **A. Hutfilz**, None; **S.R. Sonntag**, None; **B. Lewke**, None; **D. Theisen-Kunde**, None; **S. Grisanti**, None; **R. Brinkmann**, None; **Y. Miura**, None

*Alessa Hutfilz and Svenja Rebecca Sonntag contributed equally to this work.

References

1. Sparrow JR, Hicks D, Hamel CP. The retinal pigment epithelium in health and disease. *Curr Mol Med*. 2010;10:802–823.
2. Strauss O. The retinal pigment epithelium in visual function. *Physiol Rev*. 2005;85:845–881.
3. Jarrett SG, Lewin AS, Boulton ME. The importance of mitochondria in age-related and inherited eye disorders. *Ophthalmic Res*. 2010;44:179–190.
4. Schutt F, Aretz S, Auffarth GU, Kopitz J. Role of energy metabolism in retinal pigment epithelium. *Ophthalmologe*. 2013;110:345–352.
5. Schweitzer D, Schenke S, Hammer M, et al. Towards metabolic mapping of the human retina. *Microsc Res Tech*. 2007;70:410–419.
6. Dysli C, Wolf S, Berezin MY, Sauer L, Hammer M, Zinkernagel MS. Fluorescence lifetime imaging ophthalmoscopy. *Prog Retin Eye Res*. 2017;60:120–143.
7. Sauer L, Andersen KM, Dysli C, Zinkernagel MS, Bernstein PS, Hammer M. Review of clinical approaches in fluorescence lifetime imaging ophthalmoscopy. *J Biomed Opt*. 2018;23:1–20.
8. Becker W, Bergmann A, Hink MA, Konig K, Benndorf K, Biskup C. Fluorescence lifetime imaging by time-correlated single-photon counting. *Microsc Res Tech*. 2004;63:58–66.
9. Sparrow JR, Wu Y, Nagasaki T, Yoon KD, Yamamoto K, Zhou J. Fundus autofluorescence and the bisretinoids of retina. *Photochem Photobiol Sci*. 2010;9:1480–1489.
10. Nakashima N, Yoshihara K, Tanaka F, Yagi K. Picosecond fluorescence lifetime of the coenzyme of D-amino acid oxidase. *J Biol Chem*. 1980;255:5261–5263.
11. Dysli C, Wolf S, Hatz K, Zinkernagel MS. Fluorescence lifetime imaging in Stargardt disease: potential marker for disease progression. *Invest Ophthalmol Vis Sci*. 2016;57:832–841.
12. Sauer L, Schweitzer D, Ramm L, Augsten R, Hammer M, Peters S. Impact of macular pigment on fundus autofluorescence lifetimes. *Invest Ophthalmol Vis Sci*. 2015;56:4668–4679.
13. Sauer L, Andersen KM, Li B, Gensure RH, Hammer M, Bernstein PS. Fluorescence lifetime imaging ophthalmoscopy (FLIO) of macular pigment. *Invest Ophthalmol Vis Sci*. 2018;59:3094–3103.
14. Dysli C, Wolf S, Zinkernagel MS. Autofluorescence lifetimes in geographic atrophy in patients with age-related macular degeneration. *Invest Ophthalmol Vis Sci*. 2016;57:2479–2487.
15. Sauer L, Klemm M, Peters S, et al. Monitoring foveal sparing in geographic atrophy with fluorescence lifetime imaging ophthalmoscopy—a novel approach. *Acta Ophthalmologica*. 2018;96:257–266.
16. Schweitzer D, Deutsch L, Klemm M, et al. Fluorescence lifetime imaging ophthalmoscopy in type 2 diabetic patients who have no signs of diabetic retinopathy. *J Biomed Opt*. 2015;20:61106.
17. Sauer L, Gensure RH, Andersen KM, et al. Patterns of fundus autofluorescence lifetimes in eyes of individuals with nonexudative age-related macular degeneration. *Invest Ophthalmol Vis Sci*. 2018;59:AMD65–AMD77.
18. Sauer L, Gensure RH, Hammer M, Bernstein PS. Fluorescence lifetime imaging ophthalmoscopy: a

novel way to assess macular telangiectasia type 2. *Ophthalmol Retina*. 2018;2:587–598.
19. Stefansson E. Ocular oxygenation and the treatment of diabetic retinopathy. *Surv Ophthalmol*. 2006;51:364–380.
20. Zhang JJ, Sun Y, Hussain AA, Marshall J. Laser-mediated activation of human retinal pigment epithelial cells and concomitant release of matrix metalloproteinases. *Invest Ophthalmol Vis Sci*. 2012;53:2928–2937.
21. Brinkmann R, Huttmann G, Rogener J, Roider J, Birngruber R, Lin CP. Origin of retinal pigment epithelium cell damage by pulsed laser irradiance in the nanosecond to microsecond time regimen. *Lasers Surg Med*. 2000;27:451–464.
22. Brinkmann R, Roider J, Birngruber R. Selective retina therapy (SRT): a review on methods, techniques, preclinical and first clinical results. *Bull Soc Belge Ophtalmol*. 2006;51–69.
23. Klatt C, Saeger M, Oppermann T, et al. Selective retina therapy for acute central serous chorioretinopathy. *Br J Ophthalmol*. 2011;95:83–88.
24. Brinkmann R, Birngruber R. Selektive retinatherapie (SRT). *Z Med Phys*. 2007;17:6–22.
25. Kang S, Park YG, Kim JR, et al. Selective retina therapy in patients with chronic central serous chorioretinopathy: a pilot study. *Medicine*. 2016; 95:e2524.
26. Kim HD, Jang SY, Lee SH, et al. Retinal pigment epithelium responses to selective retina therapy in mouse eyes. *Invest Ophthalmol Vis Sci*. 2016;57: 3486–3495.
27. Framme C, Walter A, Prahs P, et al. Structural changes of the retina after conventional laser photocoagulation and selective retina treatment (SRT) in spectral domain OCT. *Curr Eye Res*. 2009;34:568–579.
28. Elsner H, Porksen E, Klatt C, et al. Selective retina therapy in patients with central serous chorioretinopathy. *Graefes Arch Clin Exp Ophthalmol*. 2006;244:1638–1645.
29. Yasui A, Yamamoto M, Hirayama K, et al. Retinal sensitivity after selective retina therapy (SRT) on patients with central serous chorioretinopathy. *Graefes Arch Clin Exp Ophthalmol*. 2017;255:243–254.
30. Roider J, Liew SH, Klatt C, et al. Selective retina therapy (SRT) for clinically significant diabetic macular edema. *Graefes Arch Clin Exp Ophthalmol*. 2010;248:1263–1272.
31. Richert E, Koinzer S, Tode J, et al. Release of different cell mediators during retinal pigment epithelium regeneration following selective retina therapy. *Invest Ophthalmol Vis Sci*. 2018;59:1323–1331.
32. Schmitz-Valckenberg S, Fleckenstein M, Scholl HP, Holz FG. Fundus autofluorescence and progression of age-related macular degeneration. *Surv Ophthalmol*. 2009;54:96–117.
33. Sparrow JR, Duncker T. Fundus autofluorescence and RPE lipofuscin in age-related macular degeneration. *J Clin Med*. 2014;3:1302–1321.
34. Gliem M, Muller PL, Finger RP, McGuinness MB, Holz FG, Charbel Issa P. Quantitative fundus autofluorescence in early and intermediate age-related macular degeneration. *JAMA Ophthalmol*. 2016;134:817–824.
35. Kayatz P, Thumann G, Luther TT, et al. Oxidation causes melanin fluorescence. *Invest Ophthalmol Vis Sci*. 2001;42:241–246.
36. Miura Y, Huettmann G, Orzekowsky-Schroeder R, et al. Two-photon microscopy and fluorescence lifetime imaging of retinal pigment epithelial cells under oxidative stress. *Invest Ophthalmol Vis Sci*. 2013;54:3366–3377.
37. Hammer M, Sauer L, Klemm M, Peters S, Schultz R, Haueisen J. Fundus autofluorescence beyond lipofuscin: lesson learned from ex vivo fluorescence lifetime imaging in porcine eyes. *Biomed Opt Express*. 2018;9:3078–3091.
38. Yakovleva MA, Feldman TB, Arbukhanova PM, Borzenok SA, Kuzmin VA, Ostrovsky MA. Estimation of fluorescence lifetime of lipofuscin fluorophores contained in lipofuscin granules of retinal pigment epithelium of human cadaver eyes without signs of pathology. *Dokl Biochem Biophys*. 2017;472:19–22.
39. Dysli C, Schurch K, Pascal E, Wolf S, Zinkernagel MS. Fundus autofluorescence lifetime patterns in retinitis pigmentosa. *Invest Ophthalmol Vis Sci*. 2018;59:1769–1778.
40. Dysli C, Wolf S, Tran HV, Zinkernagel MS. Autofluorescence lifetimes in patients with choroideremia identify photoreceptors in areas with retinal pigment epithelium atrophy. *Invest Ophthalmol Vis Sci*. 2016;57:6714–6721.
41. Heikal AA. Intracellular coenzymes as natural biomarkers for metabolic activities and mitochondrial anomalies. *Biomark Med*. 2010;4:241–263.
42. Nakashima N, Yoshihara K, Tanaka F, Yagi K. Picosecond fluorescence lifetime of the coenzyme of D-amino-acid oxidase. *J Biol Chem*. 1980;255: 5261–5263.
43. Walsh AJ, Cook RS, Manning HC, et al. Optical metabolic imaging identifies glycolytic levels,

subtypes, and early-treatment response in breast cancer. *Cancer Res*. 2013;73:6164–6174.
44. Meleshina AV, Dudenkova VV, Bystrova AS, Kuznetsova DS, Shirmanova MV, Zagaynova EV. Two-photon FLIM of NAD(P)H and FAD in mesenchymal stem cells undergoing either osteogenic or chondrogenic differentiation. *Stem Cell Res Ther*. 2017;8:15.
45. Alam SR, Wallrabe H, Svindrych Z, et al. Investigation of mitochondrial metabolic response to doxorubicin in prostate cancer cells: an NADH, FAD and tryptophan FLIM assay. *Sci Rep*. 2017;7:10451.
46. Skala M, Ramanujam N. Multiphoton redox ratio imaging for metabolic monitoring in vivo. *Methods Mol Biol*. 2010;594:155–162.
47. Gilmore AM, Hazlett TL, Govindjee. Xanthophyll cycle-dependent quenching of photosystem II chlorophyll a fluorescence: formation of a quenching complex with a short fluorescence lifetime. *Proc Natl Acad Sci U S A*. 1995;92:2273–2277.
48. Miura Y. Retinal pigment epithelium–choroid organ culture. *Expert Rev Ophthalmol*. 2014;6:669–680.